Journal of Geophysical Research: Oceans

RESEARCH ARTICLE
10.1029/2017JC013667

Key Points:
- An Algerian eddy was tracked for 8 months in the Mediterranean Sea revealing interactions and mass exchanges between individual structures
- The dual-core eddy was composed of a surface water mass (Atlantic Water) and a modal water mass (Western Intermediate Water)
- High-resolution sampling revealed submesoscale structures

Correspondence to:
P. Garreau,
pierre.garreau@ifremer.fr

Citation:
Garreau, P., Dumas, F., Louazel, S., Stegner, A., & Le Vu, B. (2018). High-resolution observations and tracking of a dual-core anticyclonic eddy in the Algerian Basin. *Journal of Geophysical Research: Oceans*, *123*, 9320–9339. https://doi.org/10.1029/2017JC013667

Received 5 DEC 2017
Accepted 14 NOV 2018
Accepted article online 21 NOV 2018
Published online 26 DEC 2018

High-Resolution Observations and Tracking of a Dual-Core Anticyclonic Eddy in the Algerian Basin

P. Garreau[1], F. Dumas[2], S. Louazel[2], A. Stegner[3], and B. Le Vu[3]

[1]IFREMER, Université de Brest, CNRS UMR 6523, IRD, Laboratoire d'Océanographie Physique et Spatiale (LOPS), IUEM, Plouzané, France, [2]Service Hydrographique et Océanographique de la Marine, Brest, France, [3]Laboratoire de Météorologie Dynamique (LMD), CNRS UMR 8539, Ecole Polytechnique, Palaiseau, France

Abstract Mesoscale dynamics in the Mediterranean Sea have been investigated for years, and anticyclonic eddies are regularly observed features in the Algerian Basin. Here we used the AMEDA eddy detection algorithm to track and monitor a particular anticyclonic eddy from its birth to its death. The analysis of remote sensing data sets (AVISO and sea surface temperature) revealed that this anticyclone split from an Algerian eddy, in October 2015, interacted with the North Balearic Front and merged 7 months later, in May 2016, with a similar Algerian eddy. In early spring 2016, a field experiment during the ProtevsMed 2016 cruise thoroughly investigated this eddy, when it was located near the North Balearic Front, taking high-resolution (Seasoar) hydrological transects, several Conductivity-Temperature-Depth (CTD) casts, and Lowered Acoustic Doppler Profiler measurements. In addition, four drifting buoys were released in the eddy core. These in situ measurements revealed that the vertical structure of this anticyclone was made of two water lenses of very different origins (Atlantic Water above and Western Intermediate Water below) spinning together. In the vicinity of the North Balearic Front, which may act as a dynamical barrier to such oceanic structures, the eddy interacted with a subsurface anticyclonic eddy made of modal water, which fostered cross-front exchanges generating filaments by stirring. The high-resolution sampling revealed fine-scale structures both adjacent to the eddy and within its core.

Plain Language Summary A persistent eddy was observed during a scientific cruise in the western Mediterranean Sea. Eddies are spinning water masses with particular characteristics. Using satellite data, it was possible to track the eddy for several months. Thanks to an undulating towed vehicle, the eddy studied here revealed an unexpected structure: it was formed of two superposed water masses of very different origins. The warmer water mass came from the Atlantic Ocean, and the colder one was created in the northwestern Mediterranean Sea, in winter. In this study, we explore how these different water masses joined and yet retained their individual characteristics for a relatively long time.

1. Introduction

Eddies are oceanic structures, transporting and trapping water masses and biochemical properties, shielding their core from strong mixing with the surrounding environment. Conversely, when mesoscale dynamics are intense, interactions between structures foster at small-scale exchanges between water masses at their periphery (Robinson, 1983). A major oceanographic challenge is to understand the role played by mesoscale eddies in the distribution of temperature, salinity, and biological productivity in the ocean and how they participate in the vertical exchange between the ocean interior and the surface layer (McGillicuddy, 2016; McWilliams, 2013). In the Algerian Basin, anticyclonic eddies spread Atlantic Water (AW) northward, feed the West Corsica Current, and provide potential energy to the cyclonic circulation in the northern part of the western Mediterranean Basin (Millot, 1999).

Described nearly 30 years ago by Millot et al. (1990) using infrared sea surface temperature (SST) images, Algerian eddies (AEs) are generated by the unstable meanders of the Algerian Current (Salas et al., 2003; Taupier-Letage et al., 2003; Font et al., 2004). A large number of AEs detach from the Algerian coast upstream of the Sardinian Channel (8°E) and then move in a counterclockwise manner northwestward up to the North Balearic Front (NBF), the Balearic Islands, reaching even the Almeria-Oran Front (Perez, 2003). A deep cyclonic circulation within the Algerian Basin has been demonstrated using RAFOS drifters, and two subsurface gyres were identified, centered at around 37°30′N to 2°30′E and 38°30′N to 6°00′E (Testor et al., 2005). Revisiting 20 years of altimetric data with several eddy detection algorithms, Escudier, Renault, et al. (2016) confirmed

the two counterclockwise circulations of the eddies in the Algerian Basin and identified two preferential areas of detachment from the Algerian Current within the intervals of 2–4°E and 6–8°E. The dynamics of the Algerian Basin are dominated by numerous anticyclonic eddies, filaments, and meandering. Despite intense interactions between these structures leading to merging, squeezing, or squashing processes, individual eddies can be followed for a few months and sometimes for a few years (Puillat et al., 2002). Although they may extend over a wide part of the water column (up to 1,000 m), the eddies intensify in the first 300–400 m, near the surface. The maximal azimuthal velocity of such anticyclones is about 0.4–0.6 m/s (Ruiz et al., 2002).

The anticyclonic eddies of the Algerian Basin are mainly composed of AW coming from the Algerian Current, which is a major source of eddy formation. Nevertheless, other identified water masses of the Mediterranean Sea are involved and redistributed by these mesoscale structures. Previous hydrographic surveys (Benzohra & Millot, 1995a, 1995b; Fuda et al., 2000) revealed relatively unmixed Western Intermediate Water (WIW; formerly called Winter Intermediate Water) and Levantine Intermediate Water (LIW) associated with AEs. Benzohra and Millot (1995a) discussed the origin of the WIW found under the core of a large open-sea eddy of 120–140 km in diameter just after its detachment. He suggested that the WIW is formed locally in winter by AW cooling or advected from its formation areas in the northern part of the basin. After winter, some lenses of the WIW may survive for months as modal waters called *weddies*—winter intermediate eddies—in the Balearic Basin (Juza et al., 2013; Pinot & Ganachaud, 1999). This water mass is characterized by a subsurface minimum of temperature between the AW and the LIW, deflecting the later to a deeper zone. These isolated water masses may also persist, as smaller structures, called Submesocale Coherent Vortices (SCVs; Bosse et al., 2016). They are able to move to the Algerian Basin. The exact process that associate secondary water masses (WIW and LIW) with the AEs has not yet been clearly identified.

The mesoscale patterns of eddies has been extensively observed, but the nonlinear dynamics and the interactions with the atmosphere generating finer-scale motions have mainly been explored only numerically and theoretically. Recent high-resolution numerical modeling of eddies have described submesoscale processes (Brannigan, 2016; Brannigan et al., 2017; Zhong et al., 2017). Likewise, observed eddies appear often more complex than expected. Although satellites imagery reveals spiraling in eddy cores as a surface signature of ageostrophic dynamics, the complete observation of the 3-D dynamics and associated tracer fields are incomplete. Obtained during the OMEGA-2 field experiment in November 1996 (Allen et al., 2008), high-resolution observations of a weddy in the Algerian Basin, near the Almeria-Oran frontal area, show an oblate lens of 20-km radius, 150 m thick, centered at 250-m depth, which caused anticyclonic circulation near the front, with associated currents on the order of 0.20 m/s. However, no clear connection with a surface signature of an associated AE was demonstrated. A few years later, a more obvious patch of WIW was described in the same area, and the effect of this WIW core on vertical turbulence was explored (Forryan et al., 2012). Combining gliders and remote sensing, Ruiz et al. (2009) investigated a 100-km-wide AE in the eastern Alboran Sea. They captured fine-scale structures, subducting to 120-m depth, on its edge and assessed the structure and the order of magnitude of the vertical velocity. Further to the east, Cotroneo et al. (2016) studied a 60-km-wide AE near 4°W to 38°N and described submesoscale features mainly using chlorophyll and dissolved oxygen tracers. Although the lack of horizontal resolution prevents a thorough interpretation of the results, the effects on biochemistry tracers suggested the occurrence of some submesoscale processes. Despite these recent developments in glider technology, synoptic observations of "secondary" circulation in the eddy core or periphery remains undersampled, and more thorough high-resolution surveys of mesoscale eddies are sorely needed.

The ProtevsMed 2016 cruise aimed to describe and understand the origin of the freshwater involved in the North Current and the associated large cyclonic circulation in the northwestern Mediterranean Sea, sometimes called Northern Gyre. In this context, AW bodies close to the NBF were of primary interest. Applying a very high-resolution survey, we expected to find fine-scale structures in the NBF. Serendipitously, a very singular anticyclonic eddy was present near the front, providing a unique opportunity to observe submesoscale structures revealing secondary circulations, vertical motion in the core, intense stirring in the periphery, and strong interaction with adjacent dynamical structures. This is the first dual-core eddy to be described in the western Mediterranean Sea. It was tracked from its birth by eddy splitting until its death by merging and intensively surveyed during a field experiment (section 2). Eddy tracking revealed that eddy-eddy interactions play a role in north-south mass exchanges (section 3). The high-resolution in situ observations highlight small-scale processes embedded in mesoscale eddy dynamics; the interaction of the eddy with NBF is

described (section 4). An interpretation of the process leading to this dual-core body is discussed (section 5). Finally, we summarize our results in a conclusion (section 6).

2. Materials and Methods

2.1. Eddy Detection and Tracking Using Remote Sensing Products

To investigate the temporal behavior of the mesoscale eddies in the Algerian Basin, we used the geostrophic velocity fields, produced by Salto/Duacs, distributed by AVISO, and derived from absolute dynamical topography (ADT). The *all-sat-merged* series combines, for the years 1993–2016, up-to-date data sets with up to four satellites at a given time (Pujol et al., 2016), using all missions available at a given time (Topex/Poseidon, ERS-1 and ERS-2, Jason-1 and Jason-2, Saral, Cryosat-2, and Envisat missions). This specific product for the Mediterranean Sea is projected on a 1/8° Mercator grid with time intervals of 24 hr. The horizontal resolution of the gridded velocity fields ($dX \simeq 12$ km), based on track frames, along-track filtering, and optimal interpolation, can hardly resolve the internal deformation radius Rd, which is approximately 8–15 km in the western Mediterranean Sea (Escudier, Mourre, et al., 2016). The surface signature of large mesoscale eddies with a characteristic radius that exceeds the deformation radius can generally be detected (Amitai et al., 2010; Ioannou et al., 2017; Isern-Fontanet et al., 2006; Mkhinini et al., 2014; Pascual et al., 2007; Rio et al., 2007). Nevertheless, the spatiotemporal heterogeneity of the altimetric tracks of satellites may also miss eddies or induce systematic bias on eddy intensity.

To follow the complete trajectory of the surveyed anticyclone and its interaction with neighboring eddies, we used the AMEDA algorithm (Le Vu et al., 2018). This automatic eddy detection and tracking algorithm uses a hybrid methodology based on dynamical physical parameters (local normalized angular momentum) and geometrical properties of the velocity field (closed streamlines). It quantifies the dynamical characteristics of the detected eddies and especially the mean velocity profile. When the distance to the center increases, the mean azimuthal velocity increases until a maximum value (V_{max}) is reached. A *characteristic contour*, that is, the closed streamline corresponding to the maximum azimuthal velocity, is obtained for each eddy. A typical eddy radius R_{max}, also called the *speed radius* in previous studies (Chelton et al., 2011), is then computed from the area $A = \pi {R_{max}}^2$ surrounded by the characteristic contour. However, most importantly, the tracking procedure identifies merging and splitting events. Therefore, it can better track the origin of the water masses inside the detected eddy.

2.2. In Situ Sampling Strategy

Given that the eddy was detected in mid-March, before the field experiment (Figures 2e and 2f) south of the NBF, it was targeted from 27 March to 1 April 2016 taking advantage of a meteorologically favorable period. It was sampled with

1. a towed undulating vehicle, the SeaSoar designed and built by Chelsea Instruments; mounted on either side were two Sea-Bird SBE-9 (with SBE 3 temperature and SBE 4 conductivity sensors) instruments and a chlorophyll *a* WetStar WET Labs fluorometer;
2. CTD casts performed with the Sea-Bird SBE-9 instrument and a Lowered Acoustic Doppler Profiler (LADCP, RDI 150 kHz) mounted in a General Oceanics 12-place rosette frame fitted with 12 Niskin bottles;
3. drifters with holey sock positioned at 50 m, below the expected Ekman layer. After removing spikes, raw positions were resampled hourly using a B-spline interpolation, keeping the inertial oscillations.

Unfortunately, the hull mounted ADCPs were out of order. Salinity was measured using the practical salinity scale. The towed undulating SeaSoar platform was operated with a horizontal velocity ranging from 8 to 9 knots. At this speed, the vehicle can descend to 400-m depth, allowing quasisynoptic sampling of the eddy with a horizontal resolution of about 1 nautical mile. The duration of a typical transect of 150 km took half a day, which is less than the inertial period. The sampling strategy is summarized in Figure 1. The first SeaSoar zonal transect (GT1) crossed the eddy center estimated at 4°40′E, 39°50′N. The second transect (GT2, not shown) is a transit transect outside the eddy up to its northern boundary. The GT3 transect is a meridional transect sampling the eddy from its northern edge, near the NBF, to the eddy center. Unfortunately, the vessel was not allowed to extend further south (unauthorized area). The last transect (GT5, not shown) crossed the eddy center again from the southwest to the northeast and confirmed the position of the eddy center and some cylindrical symmetry of the eddy pattern. On 29 March, nine CTD casts (numbered CTD013 to

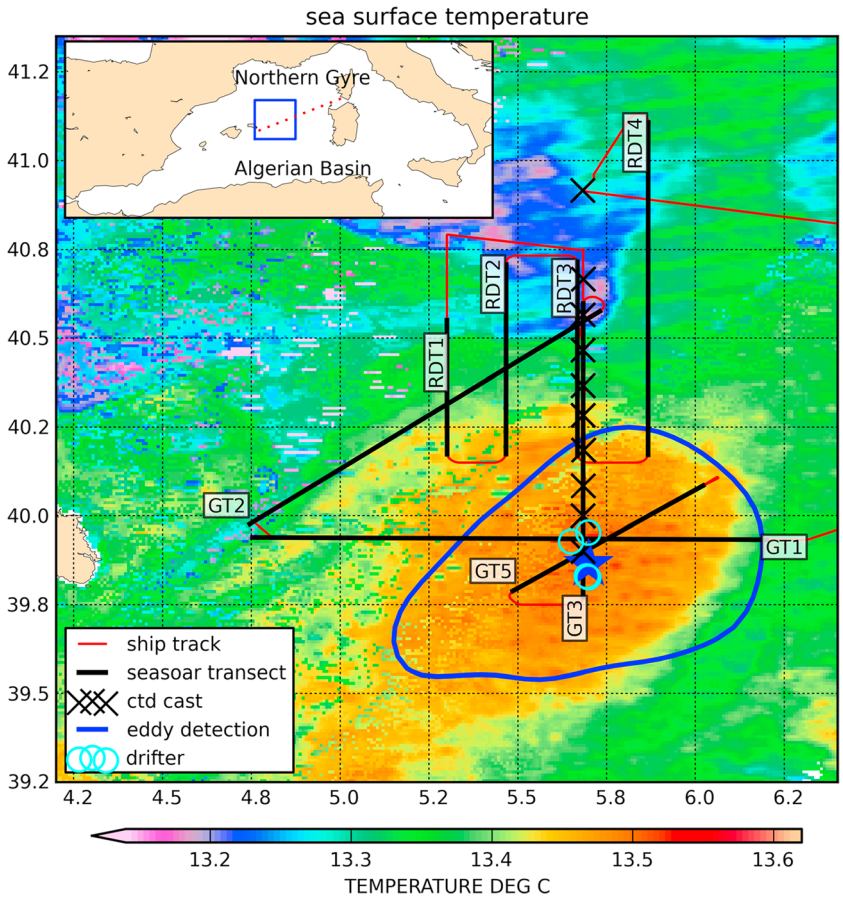

Figure 1. Eddy signatures on the sea surface temperature scene from a Metop/AVHRR/3 radiometer (29 March 2016). The eddy center (blue star) and the contour of maximum velocity (solid blue line) were both inferred from the AVISO data sets, according to the AMEDA algorithm. The SeaSoar transects are indicated with black lines. Drifter release positions are shown (light blue circles). The crosses (x) indicate CTD cast positions, and the red lines show the ship track. The situation box represents the position of the eddy in the northwestern Mediterranean Sea (blue square). The mean position of North Balearic Front is drawn (red dotted line). All in situ data were recorded from 27 March to 1 April.

CTD021 from eddy center toward the NBF) with LADCP profiles were taken along the GT3 transect to obtain additional information on deeper layers (at least down to 1,500 m). In the early morning, four drifters (with holey socks immersed at 50-m depth) were dropped successively near the estimated eddy center during the transit between CTD0013 and CDT0014. Lastly, four parallel meridional Seasoar transects (RDT1 to RDT4) were performed along the northern edge to investigate the interactions with the NBF and the possible presence of fine-scale structures. A typical profile of the northern area was then sampled by a final CTD cast (CDT022) and LADCP measurements before leaving the area at the very end of the meteorologically favorable period. The total duration of this in situ sampling was about 4 days, but the drifters remained trapped in the eddy core for approximately 1 month.

3. Eddy Detection and Tracking

3.1. The Past Trajectory of the Anticyclone: From Its Birth to the NBF

The use of the automatic eddy detection and tracking algorithm AMEDA made it possible to trace the anticyclonic eddy back in time. Besides, we also used high-resolution SST images (VIIRS/Suomi-NPP) and the trajectories of the few surface drifters located in the area to validate the eddy trajectory. The combination of these different data sets and the characteristic eddy contours computed using AMEDA are shown in Figure 2. We found that the surveyed anticyclone arose from the splitting of an AE that occurred in late October 2015. On 2 October 2015 (Figures 2a and 2b), the AMEDA algorithm clearly identified a large-scale

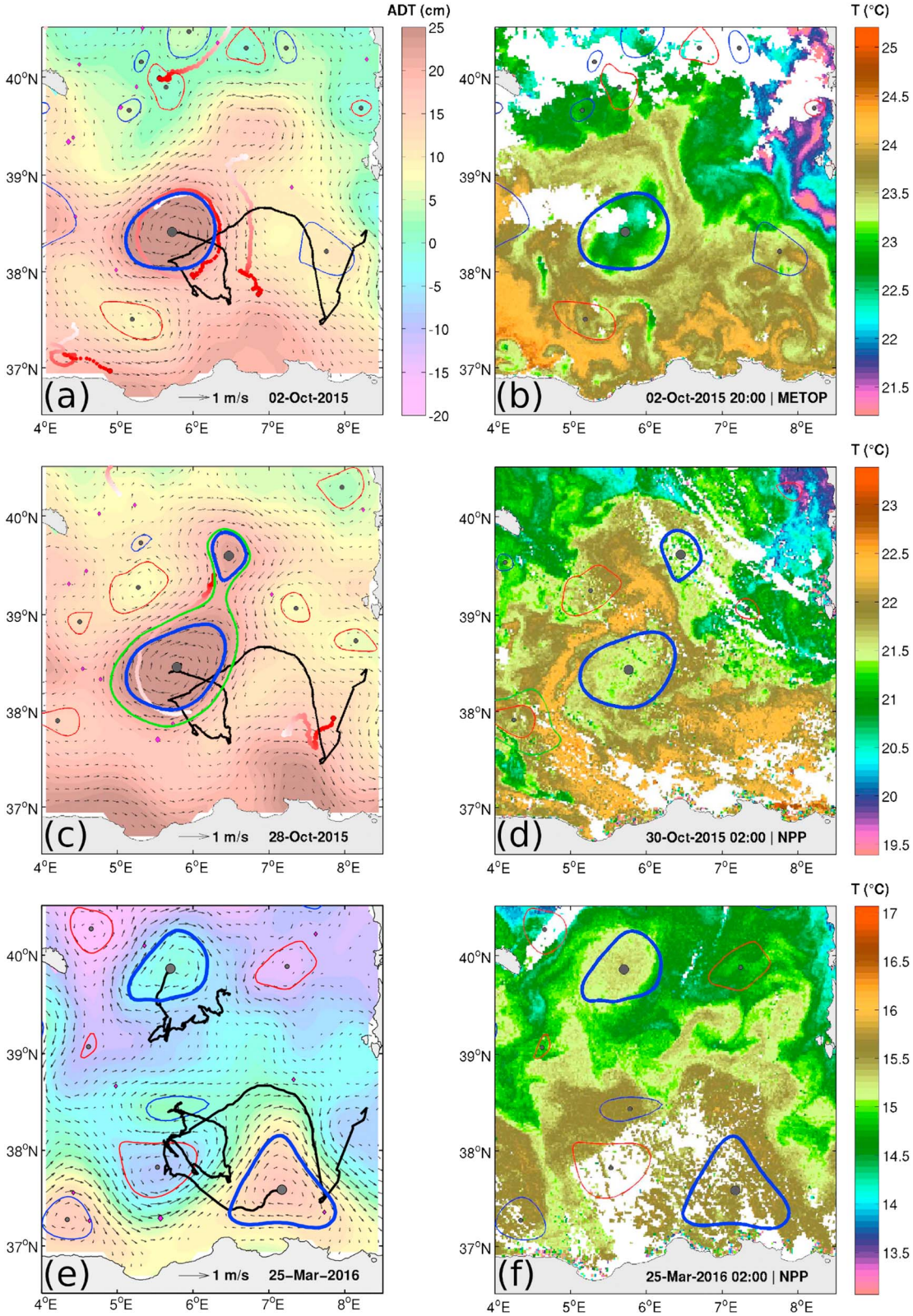

Figure 2. Eddy behavior before the field experiment. Left column: Absolute dynamical topography (ADT; color), geostrophic currents (black arrows), and characteristic contours (blue and red lines) of the eddies detected by AMEDA plotted together. The trajectories of the Algerian eddy and the surveyed anticyclone (A) are depicted by a thick black line and the positions of drifting buoys (red circles) during the previous 15 days are shown (from dark red at day 0 to white at day −15). Right column: Sea surface temperature (VIIRS/Suomi-NPP) and the characteristic contours (blue, anticyclones; red, cyclones) of the eddies detected by AMEDA.

anticyclone centered on 38.5°N 5.7°E, associated with a 25-cm ADT dome. At that time, one surface drifter (red trajectory in Figure 2a) looped around the characteristic contours of the eddy, that is, the streamline corresponding to the maximum of the mean azimuthal velocity (thick blue contour in Figures 2a and 2b). From this specific drifter trajectory, we estimated the eddy velocity V_{max} to be 30–35 cm/s and its characteristic radius R_{max} to be 50 km. These in situ measurements are in good agreement with the analysis of the AVISO geostrophic velocity field given by the AMEDA algorithm, which estimated a mean radius of R_{max} of 50 km and a maximal azimuthal velocity V_{max} of 32 cm/s for the first week of October 2015. The small Rossby number ($Ro = V_{max}/(f R_{max})$; ~0.07) corresponds to a large mesoscale eddy satisfying the geostrophic balance. The past trajectory of this anticyclone (black solid line in Figure 2) shows that it emerged from a meander of the Algerian Current, which detached from the coast at 8°E and traveled up to the Sardinian coast. This dynamical history shows that it can be classified as a typical AE. At this stage (Figure 2a), a smaller anticyclonic structure seemed to appear at its northeast edge (39.5°N, 6.8°E), but the AMEDA algorithm did not identify it as a coherent eddy having closed streamlines.

Later, on 23 October, closed streamlines began to be detected around the small anticyclone, and on 27–28 October, a *characteristic shared contour* (the green contour in Figure 2c) was identified by the AMEDA algorithm. The formation of a new eddy simultaneously with the appearance of a *characteristic shared contour* provided evidence for a splitting event (Le Vu et al., 2018). In addition, the trajectory of the drifter, which passed from the initial AE to the new anticyclone (red line in Figure 2c), confirmed the transfer of water mass between the two structures. The dynamical core of the large AE fits well with the SST patterns (Figures 2b and 2d) even if the SST signature of the small anticyclone was not as clear at this stage. However, analysis of the AVISO geostrophic currents shows that the radius of this small anticyclone grew rapidly from ~20 km on 28 October to ~40 km on 8 November. Moreover, the surface drifter made several anticyclonic loops around the new eddy center during the same period, thereby confirming the presence of the anticyclonic structure.

Four months later, a few days before the survey, this mesoscale anticyclone shifted further to the northwest following a clockwise path (Figures 2e and 2f). Its typical speed radius R_{max} was still around 40 km and associated with ADT doming reaching 15 cm. The characteristic contour of the eddy (blue line in Figure 2f) is in good agreement with the standard SST pattern of anticyclonic eddies in winter, showing a warm SST anomaly (Puillat et al., 2002). At that time, the AE had moved back to the Algerian coast following a cyclonic path in accordance with a two-gyre circulation of the eddies depicted by Testor et al. (2005) and Escudier, Renault, et al. (2016). This eddy remained coherent (it kept an anticyclonic core with closed streamlines) and interacted with the Algerian Current inducing a very large meander along the coast that propagate eastward (Figure 2e).

3.2. Merging of the Surveyed Anticyclone With the AE

The anticyclone surveyed at the end of March during the ProtevsMed 2016 cruise was detected and tracked on the AVISO data sets until 4 May 2016. On 25 April, the structure was captured by the drifters, which looped in its core (Figure 3a), and by the SST pattern (Figure 3b), which showed a cold circular anomaly with spiraling structures and stirred warm filaments especially on its north side. However, despite its relatively large size, with a diameter being larger than 50 km (according to the drifter loops), the AVISO products combined with the AMEDA algorithm did not detect the structure for 1 week. For instance, no closed streamlines were found at the eddy location on 25 April (Figure 3a). This error in detection is mainly due to the lack of altimetric tracks crossing the eddy area for almost 10 days.

The larger AE identified more southward (39°N, 7°E) is a remnant of an AE persisting since the previous November (year 2015); it interacted with the Algerian Current and partially detached from the coast during the first 2 weeks of April with similar characteristics: a 25-cm ADT dome and a characteristic radius R_{max} of around 45 km.

The monitored anticyclone (A) was detected again 1 week later, on 3 May 2016, with the altimetric analysis. The characteristic contour (blue line in Figure 3c) given by the AMEDA algorithm was slightly shifted compared with the drifter loops (Figure 3c) and the cold SST anomaly (Figure 3d). A shared characteristic contour was also identified (closed green contour in Figure 3c) on the geostrophic surface currents that encompassed both anticyclones. The subsequent disappearance of the small anticyclone indicates that the latter merged back with the AE.

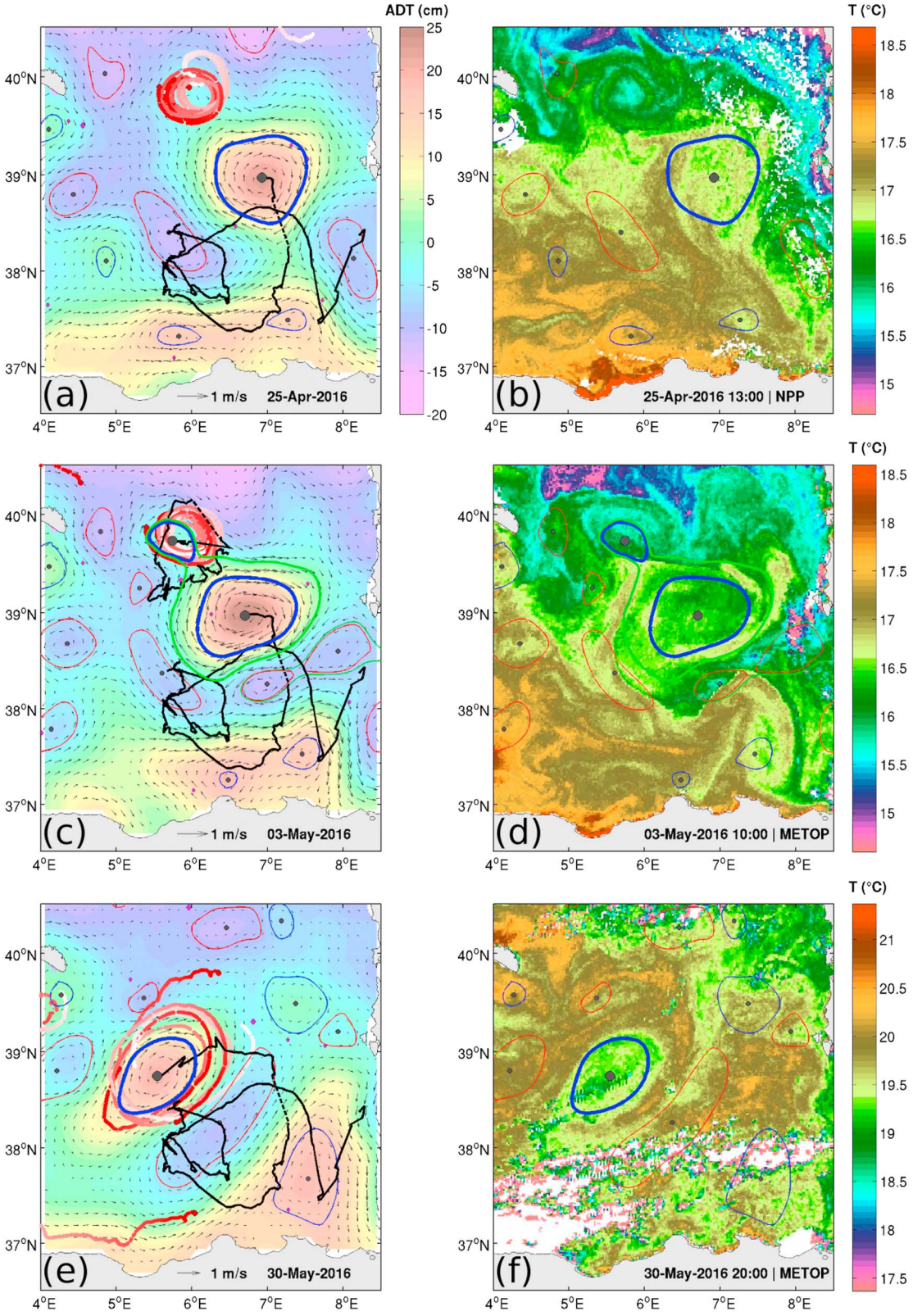

Figure 3. Eddy behavior after the field experiment. Right column: Absolute dynamical topography (ADT; color), geostrophic currents (black arrows), and characteristic contours (blue and red lines) of the eddies detected by AMEDA plotted together. The trajectories of the Algerian eddy and the surveyed anticyclone (A) are depicted by a thick black line, and the positions of drifting buoys (red circles) during the previous 15 days are shown (from dark red at day 0 to white at −15 days). Left column: Sea surface temperature (VIIRS/Suomi-NPP) and the characteristic contours (blue: anticyclones; red: cyclones) of the eddies detected by AMEDA.

This merging occurred rapidly (less than 10 days), and on 30 May (Figures 3e and 3f), the fusion was complete and resulted in a wide anticyclonic structure that captured all the drifters. This fusion confirms that the mass transfer from the small eddy to the large eddy was comprehensive. Hence, the anticyclonic eddy (A) that split from an AE in October 2015 merged back with it 7 months later.

3.3. From Warm Core to Cold Core

In winter, AEs are characterized by warm surface cores of AW in a surrounding of colder water masses. The present eddy was easily revealed before the field experiment as a warm patch on remotely sensed data on 25 March (Figure 2f). This feature persisted during the cruise experiment, and the CTD casts did not exhibit any notable surface stratification in the eddy core.

In early spring, when the downward atmosphere-ocean heat flux becomes positive again, the upper seasonal thermocline tends to reduce the horizontal gradients of the SST induced by deep mesoscale eddies. On the contrary, eddy-wind interactions lead to a total wind stress curl that favors upwelling (McGillicuddy et al., 2007). Gaube et al. (2014) showed that this upwelling is associated with weaker downwelling, forming an antisymmetric dipole in the core. Hence, both processes induce Ekman pumping inside the anticyclone and therefore reduce (or delay) surface warming. This may explain why the anticyclones A (Figures 3a and 3e) and AE (Figures 3e and 3f) appeared now as relative cold cores. Moreover, both the Rossby number (Ro = 0.13) and the relative core vorticity ($\zeta/f \sim -0.4$) of the anticyclone A reach nonnegligible values (see below sections 4.3 and 4.5), and ageostrophic dynamics (Mahadevan et al., 2008) may induce vertical mixing. The numerical simulation of Brannigan (2016) and Zhong et al. (2017), performed at very high resolution, also suggested that the surface wind stress induces ageostrophic instabilities in the mixed layer and initiates vertical mixing in anticyclonic eddies. These ageostrophic and small-scale process could also explain the relative cooling of surface water inside the anticyclone.

4. In Situ Observations and the Dual-Core Vertical Eddy Structure

4.1. Hydrographic Transects

The first transect (GT1) crossed the eddy at its center and then revealed the main properties of the eddy. It was composed of two very distinct water masses (A and A′ in Figure 4), leading to a negative anomaly of potential density. In the surface layer, the eddy was formed by a lens of AW having a salinity of less than 37.75 and a potential temperature greater than 15 °C. Near the core, the thickness of this layer reached 150 m, and the outer diameter of the eddy, estimated where isopycnals intersect the surface, was in the range of 100–125 km. Next to the eddy center, under this surface layer, a smaller hemispheric lens of cold water (less than 13.2 °C) seemed trapped under the surface structure. This water mass was also relatively fresh (salinity in the range of 37.90–38.2); it fell within the scope of WIW characteristics. The transition between the two water masses was very thin and located at a depth of 180 m. On the GT1 transect, isopycnals separating the two water masses were nearly horizontal, indicating that under geostrophic approximation, they spin together more or less at the same azimuthal velocity. Nevertheless, the GT3 transect (central panels in Figure 4) showed a small slope for the isopycnals, suggesting slight differences in azimuthal velocities.

Although this water mass did not have the typical characteristics of the WIW core (i.e., salinity between 38.1 and 38.3 and temperature less than 13.0 °C, according to Vargas-Yáñez et al., 2012), this lens was obviously the result of a similar generating process. The winter cooling of surface water in the northern part of the western Mediterranean Basin can isolate patches of fresher and colder water from air-sea exchanges, WIW, allowing them to persist below the surface layer for several months. The temperature and salinity of such patches depend on the generation area and on the intensity of winter cooling. WIW formed on the shelf of the Gulf of Lion or around the Ebro plume are fresher and colder than those formed along the offshore limit of the Northern Current or in the NBF.

In the western part of GT1 (5°E), small patches of WIW were located at 200-m depth with a temperature similar to the eddy one, but with higher salinity (between 38.3 and 38.4).

The first half of the transect from the eddy boundary southward (GT3) was very similar to the GT1 transect. In the northern part of the GT3 transect, the eddy was in contact with a subsurface cold water structure generated during the winter in the northern part of the western Mediterranean Basin. This modal structure (weddy [W] shown in Figure 4) has been repeatedly described in this area (Fuda et al., 2000; Goncharov et al., 2003)

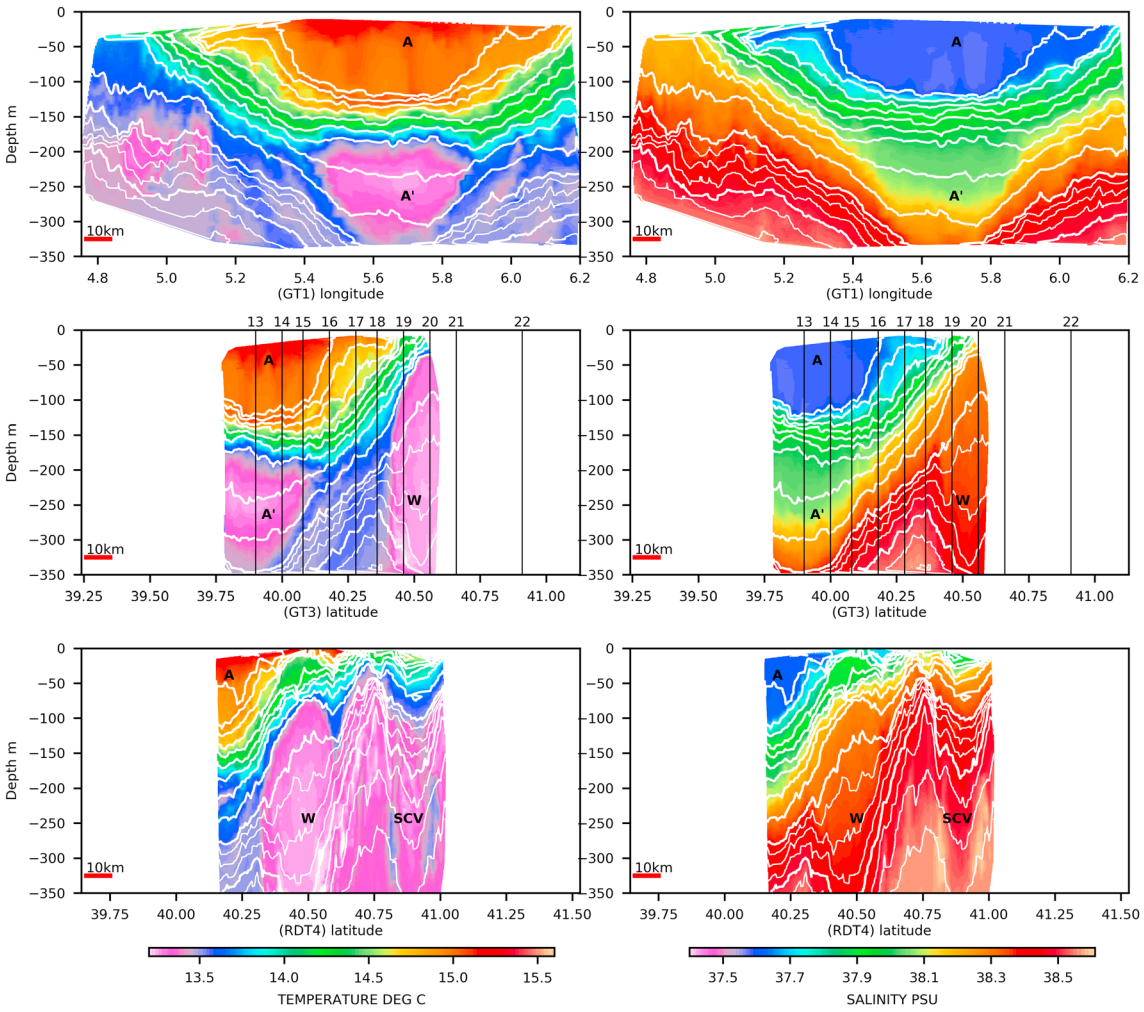

Figure 4. Temperature (left panels) and salinity (right panels) vertical cross sections along transects GT1 (28 March), GT3 (28 March), and RDT4 (30 March) from top to bottom, respectively. White lines indicate density anomalies plotted every 1 (thick) or 0.25 kg/m^3 (thin). CTD and Lowered Acoustic Doppler Profiler (LADCP) measurements along GT3 are reported (13 to 22) but not used for interpolation. AA′ indicates the surveyed eddy, W the adjacent weddy, and SCV the northernmost subcoherent vortex.

and appeared more clearly a little bit later and in a more eastward direction in the RDT4 transect. The perturbation of the isopycnal characterizes the anticyclonic behavior of the weddy (Bosse et al., 2016). Northward, near 40.9°N, an SCV induced a density perturbation down to at least 350 m. This SCV was a thin anticyclone (diameter in the range of 20 km if the transect had crossed the center). Strikingly, LIW ribbons were located on its flank with temperatures warmer than 13.5 °C and salinity in the range of 38.6 at a depth of 250–300 m. Around the eddy at 300-m depth, the top of the LIW layer displayed increasing salinity around 38.5 and temperatures in the range of 13.4–13.5 °C. Crossing the NBF northward, we therefore revealed a succession of anticyclones: an AE-like eddy (diameter of about 80 km), a subsurface weddy (diameter of about 45 km), and an SCV (diameter about 20 km), all interacting with each other.

4.2. Identification of Water Masses

The water masses present in this area were easily identifiable on the *T/S* diagram derived from CTD casts (Figure 5). Unsurprisingly, there were four of them, namely,

1. LIW characterized by an absolute maximum of salinity associated with a relative maximum temperature;
2. Western Mediterranean Deep Water;
3. AW;
4. WIWs of different characteristics.

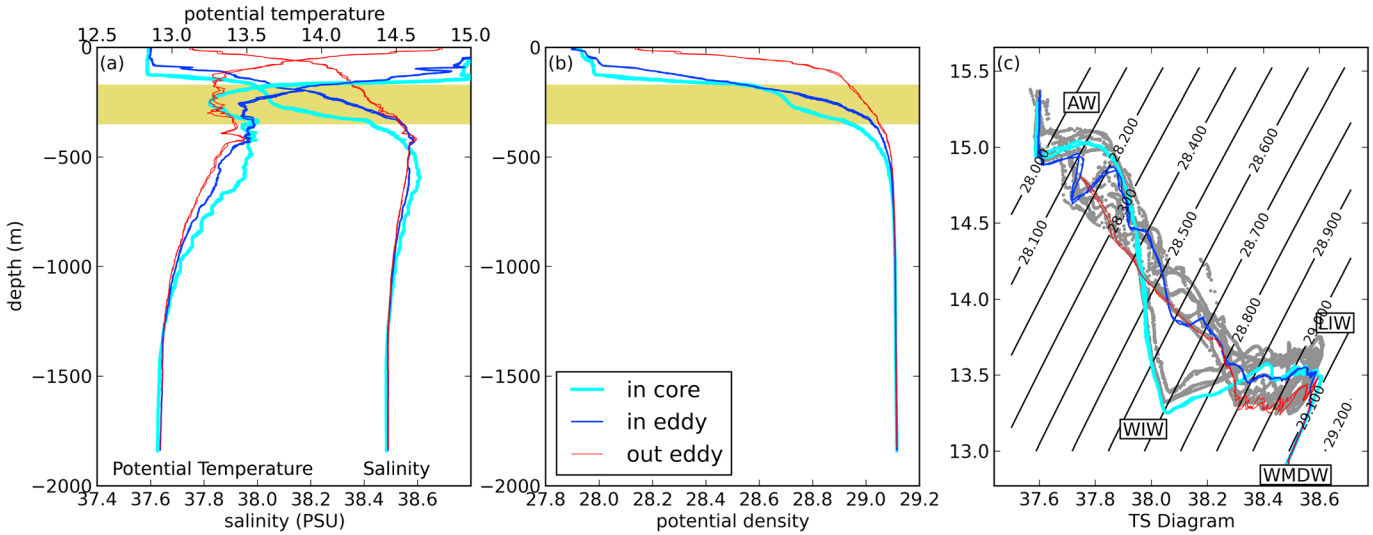

Figure 5. CTD casts along a north-south transect in the eddy. The light blue profile is located in the eddy core (CTD 14), the dark blue profile near the eddy boundary (CTD 16), and the red profile in surrounding waters (CTD 21; see Figures 1 and 4 for CTD positions). (a) Salinity and potential temperature profiles, (b) potential density, and (c) TS diagram. The green-shaded area corresponds to the WIW layer near the eddy center. The gray curves on TS diagram correspond to all other CTD cast of the transect.

The core LIW was present in the whole area between 400- and 500-m depth, even under the eddy core where the maximum of salinity was deeper (600 m), in agreement with downward convex isopycnals frequently observed under anticyclonic structures. The characteristics of the LIW in this area were a temperature around 13.5 °C and salinity of the order of 38.6 for all CTD cast profiles. Under the eddy, the LIW layer was saltier and thicker. Because the isopycnals corresponding to the LIW were convex, the rotation induced potential vorticity patterns that preserved the rotating water bodies from the surrounding environment where LIW were less marked and more mixed.

At a depth of 800 m, the eddy no longer affected the potential density, although temperature and salinity remained affected down to 1,200 m. The Western Mediterranean Deep Water characteristics showed temperatures of less than 12.9 °C and salinity of less than 38.5 in the deeper part of the profile. In the last 500 m above the seafloor, this water mass exhibited a slight increase in salinity and temperature (not shown) due to the southward migration of deep-convected water in the Gulf of Lion.

The WIW present in the eddy core appeared very clearly in the TS diagram (Figure 5), with a near-core profile showing a very marked water mass with a temperature of 13.15 °C and salinity of 38.05 °C. This isolated water mass was present only in the eddy core, but WIWs with other characteristics were present around the eddy and also appeared on the TS diagram as denser, with less marked minima of temperature and salinity in the range of 38.25–38.45.

4.3. Velocity Measurements Inside the Anticyclone

Using the high-resolution SeaSoar transect (a mean distance of 1,200 m between the rising and descending oscillation), we derived geostrophic currents from the density profiles. To do so, we assumed that the SeaSoar oscillations were vertical. The measured density profiles were then used to derive, according to the thermal wind equation, the transverse geostrophic velocity, considering the deepest level at 325 m as a zero velocity level. The geostrophic velocity section along the GT1 transect (Figure 6b) shows a surface-intensified eddy with a maximal intensity in the range of 40 cm/s in the surface layer. The eddy center, where the azimuthal velocity vanished, was estimated to be near 5.75°E, and the maximal values were reached at 5.35°E and 6.1°E. The estimated speed radius R_{max} was then around 32 km, and the corresponding Rossby number $Ro = V_{max}/(f R_{max})$, where f is the Coriolis parameter at the eddy latitude; at 40°N, $f = 0.937 \times 10^{-4}$ s^{-1} ~ 0.13. The comparison with the AVISO geostrophic velocities along the same transect is plotted in Figure 6a and shows that the meridional component of the surface velocity, derived from altimetry, corroborates the geostrophic velocity

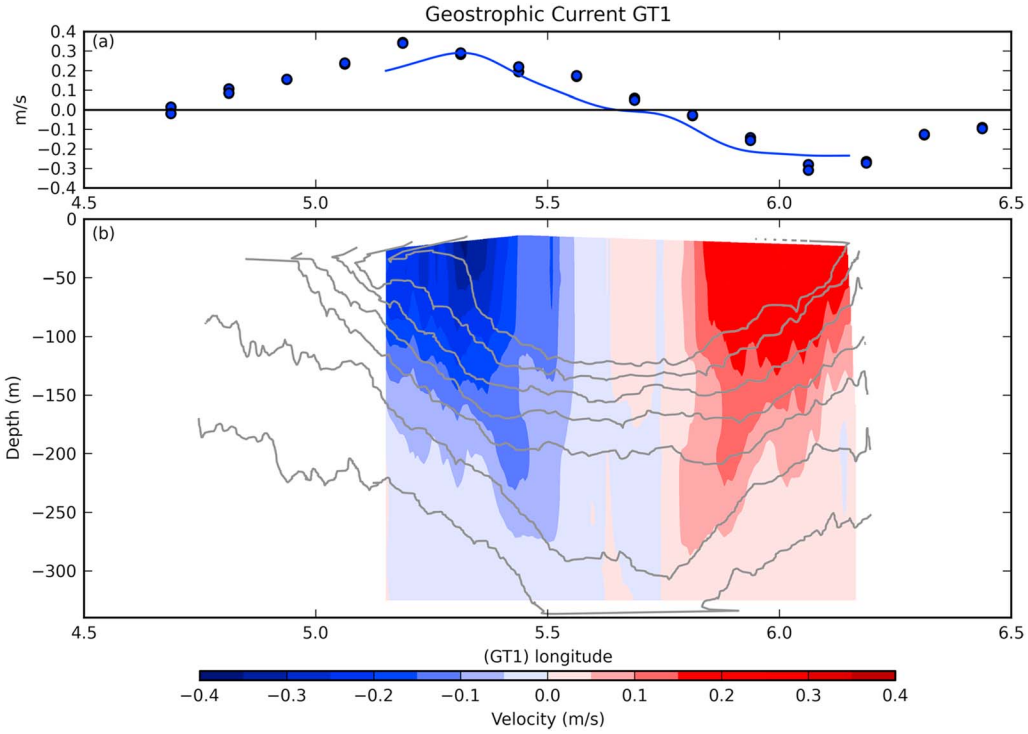

Figure 6. (a) Geostrophic velocity along the GT1 transect deduced from AVISO field derived surface slope (dots) compared with geostrophic velocity at 50-m depth deduced from density field with a reference level at 325 m. (b) Geostrophic velocity along the GT1 transect.

(at 50 m), derived from the thermal wind equation. However, as discussed in section 2.1, the characteristic speed radius R_{max} appears to be overestimated in the AVISO data set.

On the GT3 transect (half the north-south diameter), two independent velocity estimations were performed (Figure 7). First, the zonal (azimuthal) current was interpolated from 10 LADCP measurements taken during the CTD casts. Second, the zonal geostrophic velocities were estimated from the GT3 SeaSoar transect with a reference level of 360 m. The zonal geostrophic current was also derived from the CTD profiles with a more reliable reference level of 1,500 m (not shown). All velocity estimations exhibited the same pattern and roughly the same amplitude (up to 40 cm/s), thereby corroborating these independent velocity evaluations. The center of the anticyclone was estimated at around 39.9°N, and the eddy extended up to 40.5°N with surface-intensified velocities.

A secondary intensified region corresponded to the WIW lens between 160- and 300-m depth. On the LADCP data, the rotation axis (A′) of the WIW lens was not aligned with the rotation axis (A) of the AW lens and appeared to be shifted southward. This feature was confirmed by the SeaSoar-estimated velocities that showed the same behavior near the core as in the GT1 transect.

Under the surface eddy boundary, the zonal current revealed a secondary circulation pattern at the subsurface, at a depth greater than 100–150 m. At 40.45°N, the current flowed westward driven by the anticyclone of modal water (W), centered at 40.55°N described above (Figures 4b and 4c).

4.4. Interaction With the NBF

In March, the eddy moved northwestward until it reached the Balearic Front and interacted with the colder water located behind the front. The two anticyclonic structures A and W likely interacted with each other, as revealed by the vertical shear located at 40.4°N and at a depth of 75 m on the LADPC recorded velocities (Figure 7a). Using kriging techniques, an approximation of the horizontal temperature field at 75-m depth was deduced from all the Seasoar transects (Figure 8a). The anticyclonic eddy (A) was identified at 75 m deep by a patch of warm water centered near 5°40′W, 39°55′N; the second anticyclone (W) appeared as a cold (and

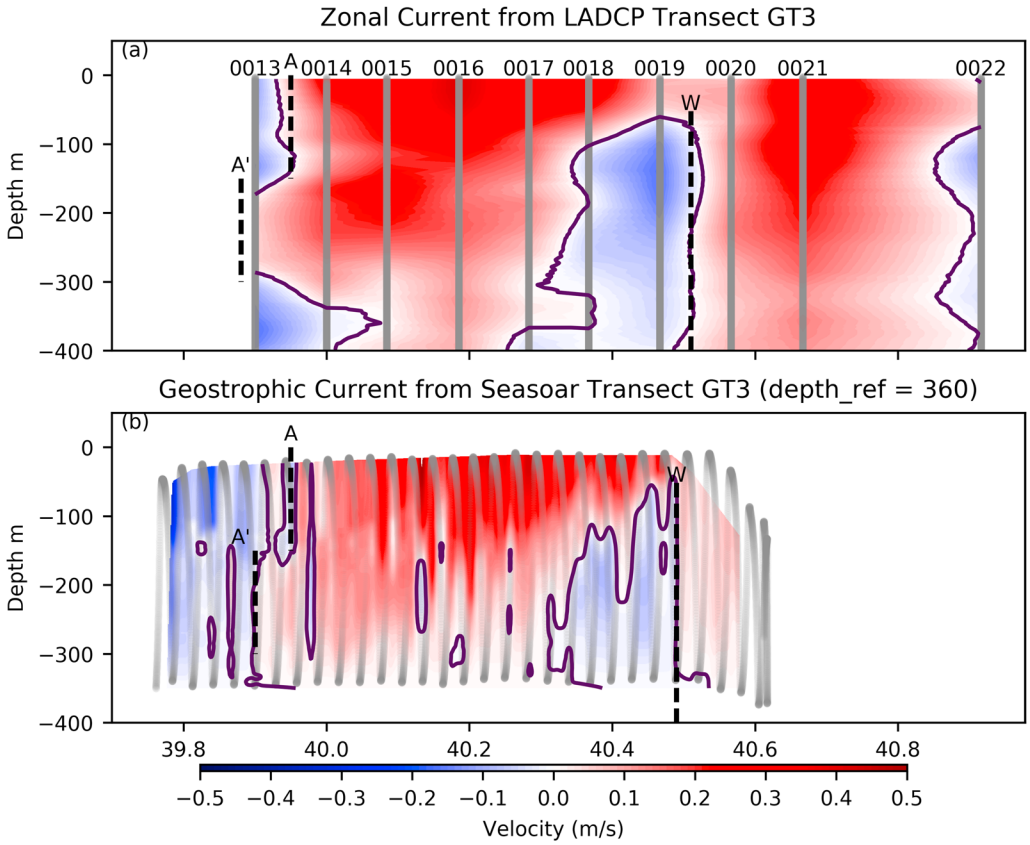

Figure 7. Velocities along the north-south transect (GT3) deduced from direct measurement by Lowered Acoustic Doppler Profiler (LADCP) (a) and from the thermal wind equation using the SeaSoar transect with a reference depth of 360 m (b). CTD and LADCP stations are designated from 0013 to 0022.

smaller) patch centered near 5°40′W, 40°30′N and was a modal structure composed of WIW. The 10 direct LADCP velocity measurements at 75-m depth were interpolated along the 5°40′N (GT3) transect and indicated that some of the subsurface eddy water mass was caught by the weddy-induced circulation. Above the modal water vortex W, an anticyclonic wrap of surface AW was trapped by the weddy and detached from eddy A (Figure 8b). Evidence for this process was also clear on the RDT4 transect (Figure 4); the AW wrapped over the weddy appeared on the surface near 41°N as warm and fresh water filaments. Weddies are ubiquitous, at least during winter and spring in the NBF, and often appear as cold-core anticyclones on remotely sensed SST data, for example, during the cruise for the month of March 2016 (x in Figure 8b). This eddy-weddy interaction leads to a net transport of AW across the NBF, giving some buoyancy to the Northern Gyre and feeding, with the West and East Corsica Currents, the density dynamics of the northwestern Mediterranean Basin.

4.5. Lagrangian Velocities and Drifting Buoys

To estimate the rotation within the eddy core and the drifting speed of the anticyclone, four SVP-type drifters, with a 50-m depth holey sock, were dropped near the eddy center on 29 March. The four drifters remained trapped in the eddy for almost 1 month with very similar trajectories (Figure 9a). The average rotation period deduced from the latitudinal or longitudinal displacement (Figures 9c and 9d) was in the range of 4 days. The Lagrangian velocities varied from 0.1 to 0.7 m/s with a mean value of around 40 cm/s after 4 April (Figure 9b). Early May, the drifters exited from the surveyed anticyclone and were caught by the larger AE located south as shown in the eddy tracking (Figure 3).

Given that the tracks were elliptic and the horizontal flux was assumed almost nondivergent, the drifter velocities increased when crossing the semiminor axis (northernmost or southernmost position) and decreased

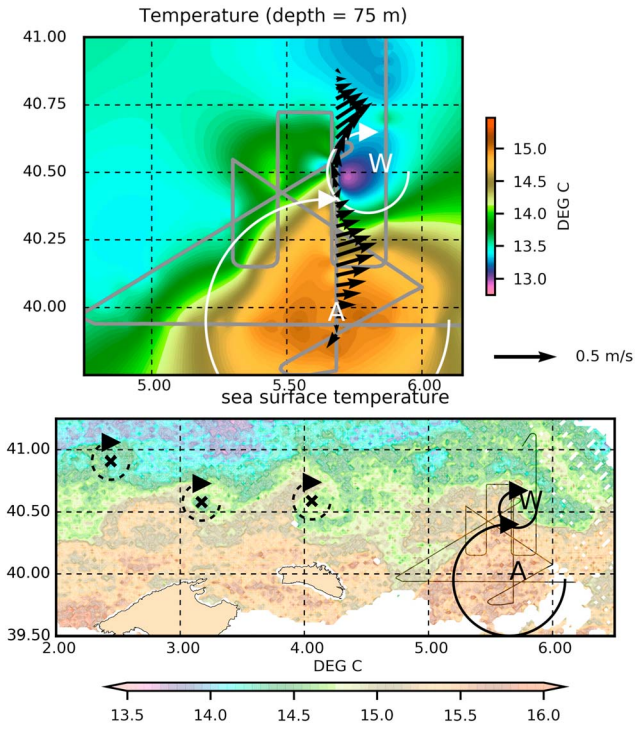

Figure 8. (a) Temperature at 75 m. Gray lines are positions of data taken into account for kriging. Currents at 75 m were interpolated from Lowered Acoustic Doppler Profiler measurements. (b) Sea surface temperature on 30 March 2016. The positions of suspected weddies, associated with clockwise surface Atlantic Water advection, are indicated (x and dashed arrows).

when crossing the semimajor axis (westernmost or easternmost position). Moreover, at the beginning of the track, drifters were closer to the eddy center and obviously moved slower (0.1–0.2 m/s). All drifters decelerated on 9 April when the eddy rapidly drifted southward and then eastward.

Assuming the eddies are ellipses that vary continuously in size, shape, and position, it is possible to extract geometrical properties of the track as instantaneous virtual streamlines from the *x*-*y* displacements of drifters (Brassington, 2009; Lilly & Gascard, 2006; Paillet et al., 2002). Therefore, the mean (averaged over one rotation period) position and velocity of the eddy center are available as the mean velocity or mean distance of the drifter from the idealized eddy center.

The four buoys drifted away from the center during the five first days. The mean radius increased, indicating a divergence in the surface layer (Figure 9e), and the radial velocity was approximately 0.04 m/s The drifters remained trapped inside the eddy for 1 month at a radius of 24 km, corresponding to the size of the homogeneous AW layer at 50-m depth (the mean depth of the holey sock). The ratio of the mean azimuthal velocity with respect to the mean radius was nearly constant for drifting buoys in the eddy (Figure 9f). For all drifters, the slopes of V_{mean} plotted against R_{mean} remained almost constant in the eddy core, with a value of around $0.18\ 10^{-4}\ s^{-1}$ (e.g., a mean azimuthal velocity of 0.40 m/s for a mean radius of 22 km). The eddy ellipticity ε was deduced from the drifter trajectories and remained weak $\varepsilon \sim 0.2$. Hence, assuming a quasicircular shape, we estimated the relative core vorticity at $\zeta_0/f = 2V_{mean}/(f\ R_{mean}) \sim -0.42$, with $f = 0.937 \times 10^{-4}\ s^{-1}$. According to this value (greater than the critical value $\zeta_0/f = -1$), the potential vorticity remained positive, and this mesoscale anticyclone cannot be affected by unstable inertial perturbations (Kloosterziel et al., 2007; Lazar et al., 2013). It may therefore remain stable and coherent for several months. Nevertheless, the negative core vorticity was not negligible and the eddy was at the limit of validity for the geostrophic balance. The centrifugal terms were no longer negligible, and some secondary ageostrophic dynamics (Mahadevan et al., 2008) may occur.

The azimuthal velocity profile derived by the AMEDA algorithm from the AVISO geostrophic velocities (gray curve on Figure 9f) underestimated the in situ drifter velocities. Similar underestimation of surface currents derived from gridded altimetric maps in comparison with in situ measurements has been reported for the North Atlantic (Fratantoni, 2001), the Alboran Gyre (Juza et al., 2016), and the Ierapetra anticyclone (Ioannou et al., 2017), due to filtering, smoothing, and optimal interpolation of altimetric data. The position of the eddy center inferred from the AMEDA tracking tools corresponds to that deduced from the drifting buoy analysis (Figures 9a, 9c, and 9d). When the eddy moved eastward (between 15 and 25 April), it escaped for 10 days the altimeter tracks, and thus, optimal interpolation and no positions were calculated.

4.6. Observation of Submesoscale and Fine-Scale Structures

SeaSoar transects and vertical profiles showed fine-scale structures inside or around the eddy exhibiting secondary motions at small scales, below the deformation radius. Already observable in hydrological transects (Figure 4), some small vertical-scale features can be highlighted by drawing the nondimensional spice variable defined as

$$s = \alpha(T - T_0) + \beta(S - S_0),$$

where α, β, T, and S are, respectively, the thermal expansion coefficient, the haline contraction coefficient, the potential temperature, and the salinity of seawater. S_0 and T_0 are reference temperature and salinity. Spice behaves as a passive tracer and can reveal secondary circulation patterns not directly driven by the mean density field. This variable highlights the submesoscale structures inside and around eddies (L'Hégaret et al., 2016; Pietri & Karstensen, 2018).

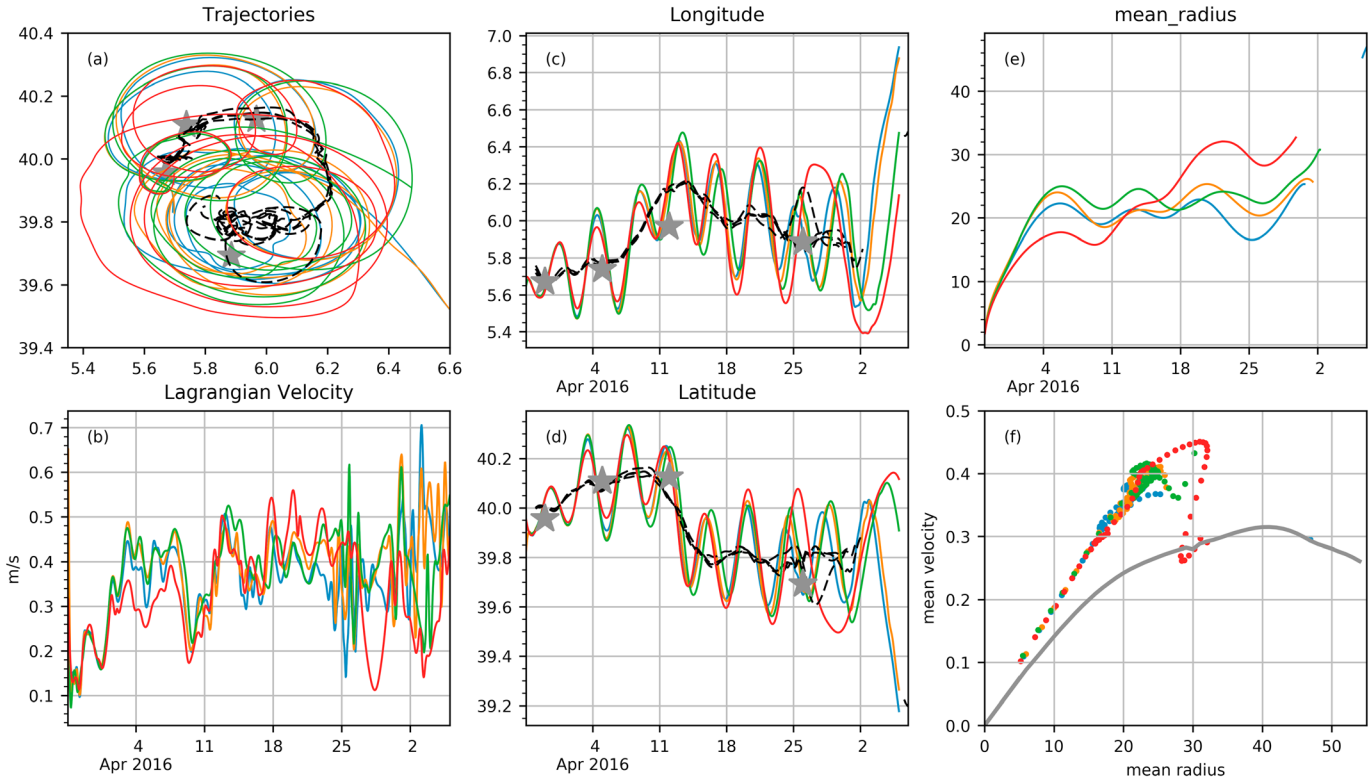

Figure 9. (a) Trajectories of the drifters dropped near the eddy core; dashed lines represent the track of the eddy center. (b) Lagrangian velocity experienced by the drifters from 29 March to 5 May; black dashed lines represent the velocity averaged over a rotation period. (c) Longitudinal and (d) latitudinal displacement of the drifters; the dashed line represents the motion of the eddy center. (e) Mean radius averaged over a rotation period. (f) Mean azimuthal velocity against mean radius. Colored lines denote the four dropped drifters; gray curve in (d) is the characteristic of the eddy deduced from AMEDA for 31 March. Gray stars on (a), (c), and (d) denote the eddy center inferred from AMEDA tracking tool.

Inside the eddy core, in the AW layer just below the surface Ekman layer, three or four cells of less spicy water were detected between 50 and 120 m deep (blue dots in Figure 10a). These cells corresponded also to patch of chlorophyll *a* (Figure 10b). They are separated by vertical plumes of more spicy water and of lower biological productivity. This particular pattern, already revealed on the temperature field and less obviously on the salinity field (Figure 4), was robust. These cells were similarly present on all other transects, suggesting a horizontal annular or spiraling shape. Vertical exchange between the top and the bottom of the eddy core is obvious, but the spice isopleths did not follow the isopycnals, and there is no evidence for intense convection. Assuming the eddy cores were not exactly in solid rotation, stirring of the upwelling/downwelling dipole may lead to this pattern. Alternatively, these observations are consistent with a study that showed, based on measurements and modeling, small-scale variations in strain, divergence, and vorticity in the eddy core (Zhong et al., 2017). A numerical study (Brannigan et al., 2017) showed similar vertical structure of a passive tracer in the eddy core with a decrease in grid size to 250 m. Both studies attributed the small-scale vertical structures to mixed layer instability and ageostrophic dynamics.

The second striking small-scale observations involve the *arms* encompassing the WIW part of the eddy and more noticeable at its western boundary. These structures were also present in other eddy transects. The arms (plumes of more spicy water denoted a-a′, b-b′, c-c′, d-d′, and e-e′; Figure 10) clearly crossed the isopycnals and were roughly aligned on an azimuthal velocity gradient (see Figure 6). Therefore, passive stirring by the geostrophic velocity field may be involved. Due to the horizontal gradients of seawater properties (the NBF) or in the presence of patches of different water masses, the shear of azimuthal velocity can generate layering aligned on a velocity gradient. A study on the layering formation in a modal structure suggests that the variability due to vortex instabilities is able to initiate the stirring process, leading to the prediction that layering under surface-intensified vortices occurs (Meunier et al., 2014).

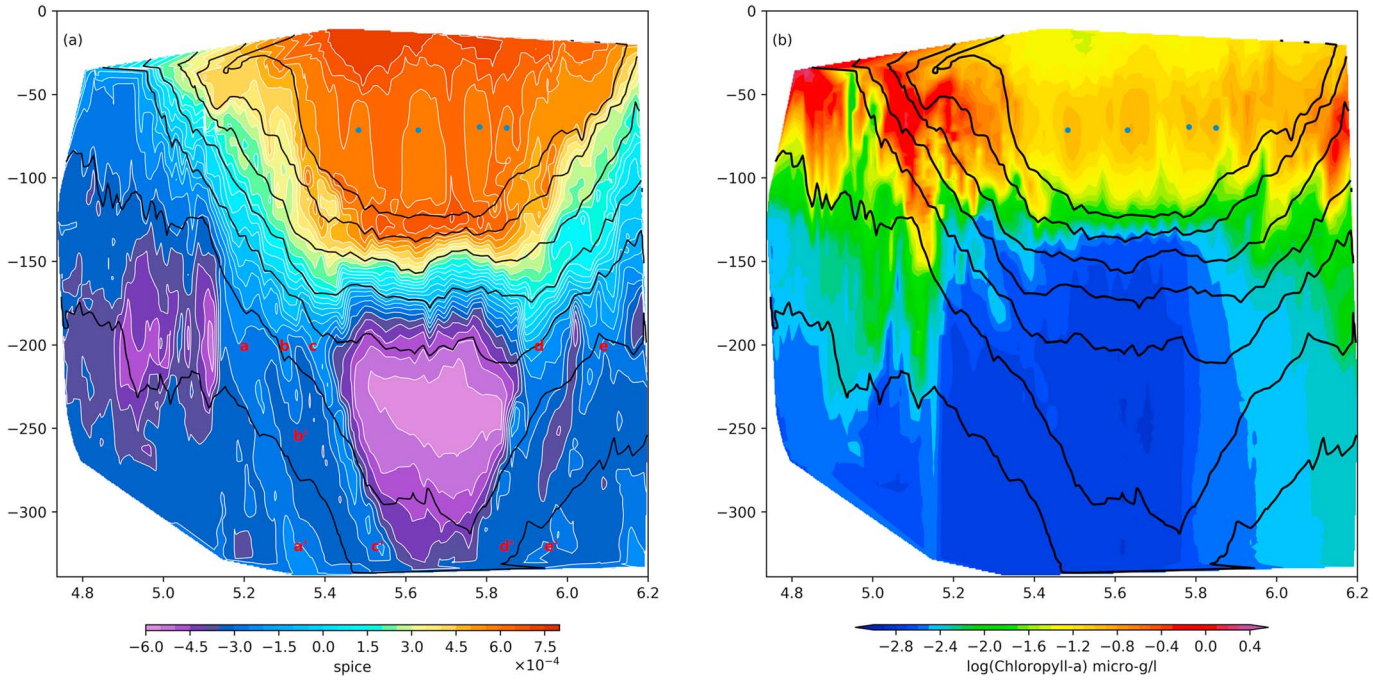

Figure 10. Nondimensional spice variable (a) and decimal log of chlorophyll *a* (b) along the GT1 transect.

Patchiness of phytoplankton also revealed submesoscale processes in the surface and subsurface layers. Fluorescence is a proxy for the estimation of chlorophyll *a* concentrations and phytoplankton abundance (Figure 10b). Inside the eddy core, the phytoplankton was strictly confined to the first 150 m, corresponding to mixed and ventilated AW layer, with a subsurface maximum located at around 75-m depth. Patches of phytoplankton corresponded to spice structures. Dynamically isolated from the surface and located under the euphotic layer, the core of WIW is logically not involved in primary production. In contrast, the eddy boundaries, where isopycnals outcrop, were in an area of stronger primary production generated by vertical fluxes of nutrients and phytoplankton. Among the processes involved, the interaction of the eddy velocity and structures with wind stress and air-sea exchanges may generate symmetric instabilities leading to a spatial succession of upwelling and downwelling along the frontal area (Brannigan, 2016). The observations in the present eddy are in agreement with these hypotheses, because the plumes of phytoplankton were found along isopycnals near the eddy boundaries.

The CTD casts 14 and 15 were both located in the core, along the GT3 transect where the two components of the eddy (AW and WIW) lenses were superimposed (Figure 11). As expected, the Brunt-Väisälä frequency was very high (greater than *f*) between the two water masses, thereby inhibiting vertical exchange of salt, heat, and momentum and preserving the two-layer structure of the anticyclone from diapycnal mixing. The thickness of this layer was roughly 50 m (yellow-shaded area in Figure. 11). Vertical profiles of current were recorded with the LADCP. The data collected during the raising and lowering of the current profiler show striking features in this transition area. The zonal velocity (here the azimuthal velocity in the eddy frame) was weaker than that of the two adjacent water masses. On CTD 14, the azimuthal velocity even vanished in this zone. This azimuthal velocity was not exactly identical in the AW and WIW lenses, as already suggested by the velocity estimations (Figures 6 and 7). The current in the deeper structure was slightly stronger. The meridional velocity (here the radial velocity in the eddy frame) remained weak or nil as expected in classical eddy models but reached a maximum in the area of increased Brunt-Väisälä frequency. The current veering suggests that this layer acts as an Ekman layer between the two water masses spinning together in the same way but with different velocities and probably misaligned rotation axes. The two parts of the eddy were dynamically uncoupled in terms of heat, salt, and momentum exchange.

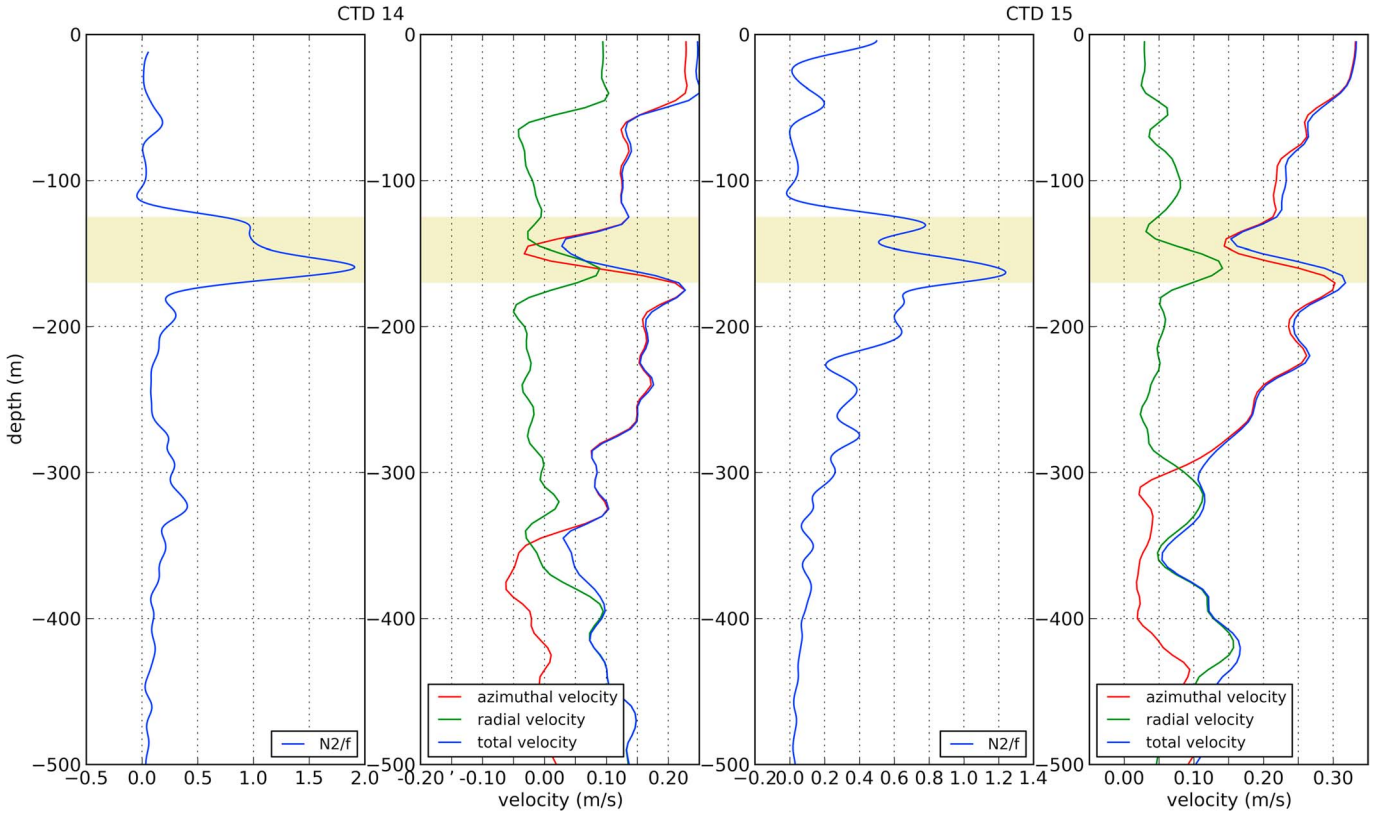

Figure 11. Brunt-Vaïsälä frequency (*N*/*f*) and velocity profile from Lowered Acoustic Doppler Profiler (LADCP) measurements in the eddy core for CTD 14 and CTD 15 (see Figures 4 and 7 for position). The yellow-shaded area corresponds to the transition layer between the Atlantic Water and the Western Intermediate Water parts of the eddy.

5. Discussion: Where Does the Cold Subsurface Water Inside the Anticyclone Come From?

As shown above, the surface layer of eddy AA′ was clearly formed from AW, which regularly stays in the Algerian Basin, south of the NBF. The WIW found below the AW was formed in the northern part of the Algerian Basin, north of the NBF. This unexpected cold patch embedded under a relatively typical eddy required further investigation.

We explored all Argo float data (35,529 profiles), glider data (72,007 profiles), CTD casts (3,621 profiles), and thermosalinograph transects available for the western Mediterranean Sea in the Coriolis database (http://www.coriolis.eu.org). Looking for the water mass encompassing all types of WIW (potential temperature less than 13.2 °C; salinity less than 38.2) showed that WIW masses were found at various depths (mainly at 20–50 m) in the Gulf of Lion, in the North Current, north of the Balearic Islands, and along the NBF (Figure 12). In the southern part of the basin, WIW was sporadically found deeper, between 120 and 250 m, as modal waters. Two paths of southward migration of WIW appeared in the data: the first path goes through the Ibiza Channel as already discussed by Pinot and Ganachaud (1999); the second path crosses the NBF east from Minorca as modeled by Juza et al. (2013).

There are at least three processes that may be involved in the formation of this singular structure.

The first process assumes that WIW is already present under the Algerian Current, as sporadically observed (Benzohra & Millot, 1995a, 1995b) and is caught by the eddy during its formation. Thereafter, this double eddy follows a typical path until it reaches the NBF, east of Minorca Island. However, despite one unique report, WIW is generally not found close to the Algerian coast.

Second, the formation of WIW during winter is not the result of classical convection generated by static instability leading to vertical motion in convective plumes, thereby enhancing strong vertical and

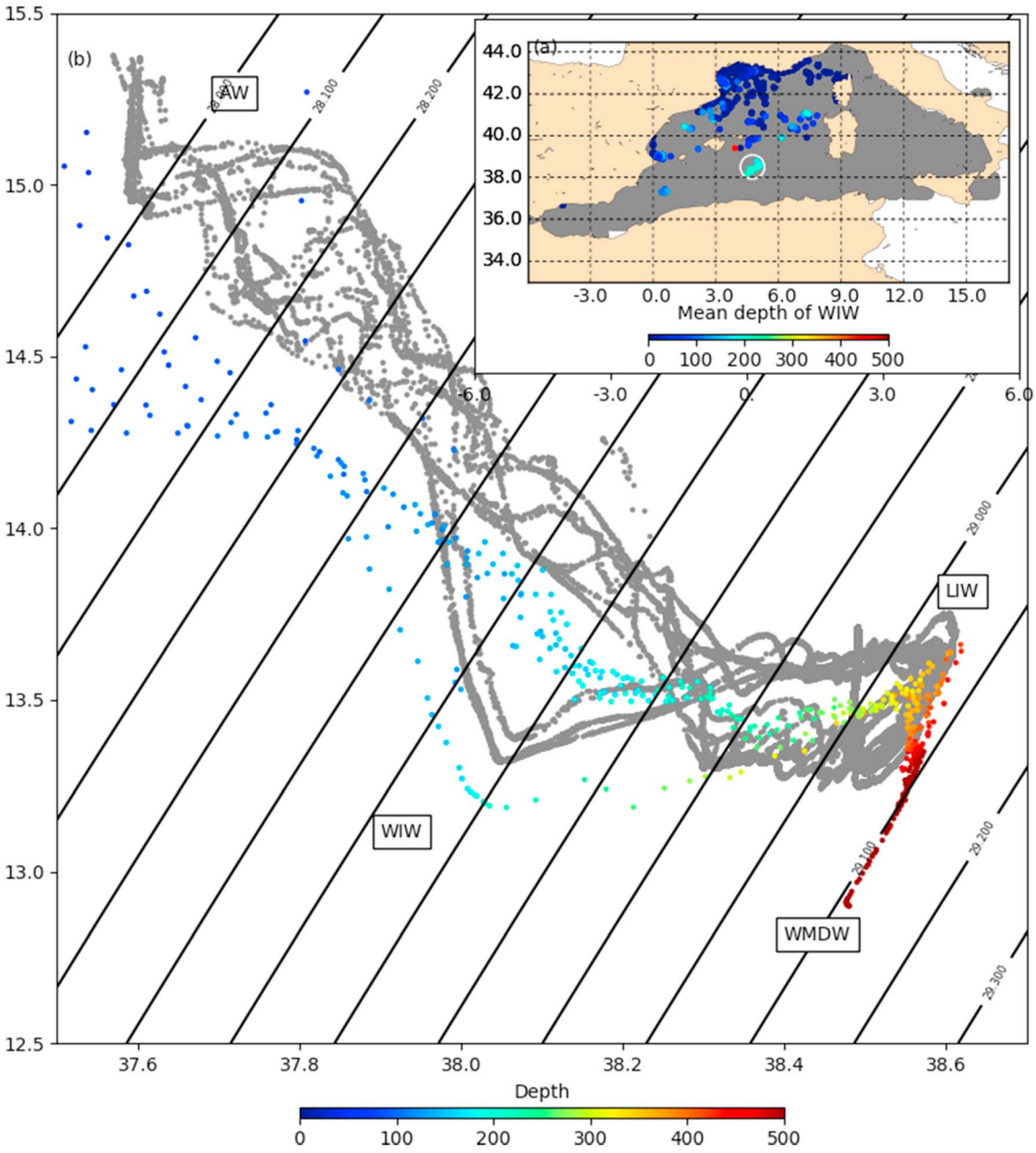

Figure 12. (a) Argo drifters, CTD, glider profiles, and surface thermosalinograph positions in the western Mediterranean Sea from 1995 to 2016 (gray dots) in the Coriolis database. When Western Intermediate Water (WIW; potential temperature $<$ 13.2 °C and salinity $<$ 38.2) is present, the mean depth of this water mass layer is shown. (b) Temperature-salinity diagram from an ARGO profiler at 38.2°N 5°E in July 2015 (white circle), and gray dots are the TS diagrams of the CTD casts in the eddy recorded in March 2016. AW = Atlantic Water; LIW = Levantine Intermediate Water; WMDW = Western Mediterranean Deep Water.

horizontal mixing. Instead, WIW appears to plunge along the isopycnal surfaces and preserve the characteristics of its water mass, involving a symmetric instability process. The main part of the WIW is known to be formed by frontal dynamics along the North Current and the Balearic Fronts. Nevertheless, in this context, anticyclonic eddies in the NBF are particularly predisposed to subduction processes as isopycnals outcrop. The WIW may plunge under an anticyclonic eddy in the Balearic Front during strong convection events (mistral gusts in February or March), as observed during the last HYMEX experiment, in glider tracks in 2013 (see Figure 6 in Estournel et al., 2016). However, winter 2015–2016 was too mild to generate such WIW characteristics (no sufficiently low temperatures were recorded by infrared images). Therefore, although this process deserves mention, it cannot have occurred for this eddy.

The third process assumes the vertical alignment of an Algerian surface eddy formed from AW with a subsurface weddy, formed from WIW. Weddies are frequently observed north of the NBF and are found to move toward the Algerian Basin across the Balearic Straits. Although a few recent eddy tracking algorithms have detected merging events between surface eddies (Le Vu et al., 2018; Li et al., 2016; Yi et al., 2014), the merging or alignment between a surface eddy and a subsurface lens cannot usually be detected with remote sensing observations. Hence, such vertical alignment can happen even if we have no evidence of its creation.

The coalescence of two anticyclonic structures has rarely been observed in situ. Cresswell (1982) demonstrated the coalescence of two anticyclonic eddies having different thicknesses and depths along the southwestern coast of Australia. The water mass of each structure was characterized during the first cruise leg and retrieved in the final structure during the second leg. The CTD cast in the final anticyclone exhibited a dual-core structure similar to the one we observed here. In the same area, Baird and Ridgway (2012) described dual-core eddies formed on the surface by water from the unstable East Australian Current and in subsurface by denser water from Bass Strait. In a stratified rotating flow, anticyclonic vortices of different densities tend to align vertically (Nof & Dewar, 1994), further supporting this assumption of vertical alignment of two separate structures.

Interestingly, the careful examination of all profiles available in the northwestern Mediterranean Sea in the Coriolis database revealed only one series of TS profiles from an SCV that is consistent with the WIW characteristics present in the lower layer of the eddy (Figure 12b). It was found in the Algerian Basin (5°W, 38.5°N) in July 2015, 8 months before our observation in March 2016, in an area affected by the dynamics of the larger southern AE (Figure 2). Unfortunately, no surface signature in sea surface height nor in SST was associated with this internal structure, and the profiles did not show any surface density anomaly related to surface structure. This SCV is nevertheless a good candidate for an alignment with a surface AE in the Algerian Basin, providing further support for the assumption of a coalescence process.

6. Conclusions

A high-resolution survey of an AE revealed an unexpected, dual-core eddy. Under the AE surface composed of AW, we found a coherent WIW water mass. These two water masses that rotate together in the same dynamical structure are not coupled by friction.

Tracking this surface eddy from its birth—upon splitting from a bigger AE—to its death—upon merging—and examining all Argo drifters available in the western Mediterranean Sea, revealed an SCV in the Algerian basin, close to the past eddy trajectory, with the appropriate WIW characteristics. Our investigations suggest that an alignment of this SCV with an AE is the origin of this dual-core eddy.

AEs composed of AW have been also associated with westward transportation of LIW in the Algerian basin. Because LIW exists as modal structures in the western Mediterranean Sea, the same vertical alignment with LIW can be expected.

Using high-resolution sampling, submesoscale features have been pointed out in observations, related to stirring when aligned on geostrophic velocity gradients or related to symmetric instability when aligned on outcropped isopycnals. The processes leading to the submesoscale observations described in this study are still under debate. Unfortunately, the lack of fine-scale azimuthal and radial velocity measurements hinders any further data interpretation. We illustrated that it is possible to carry out synoptic and in situ measurements of the submesoscale structure. More simultaneous measurements at both mesoscale and submesoscale should be generalized in future campaigns in order to validate and tune numerical simulations of the internal eddy dynamics at very high resolution.

The NBF not only is a surface and seasonal front but also clearly separates the Algerian Basin from the Northern Gyre dynamics. Nevertheless, this front is not hermetic, and mesoscale processes can enhance cross-front exchanges. Due to partial convection and surface water subduction, anticyclones also stay in the northern and denser part of the front as modal water structures. Called weddies, or SCVs when smaller, such winter-formed water migrates toward the NBF and sometimes penetrates the Algerian Basin. Close to the front, they are able to catch surface AW and then bring buoyancy to the general cyclonic dynamics encompassing the northwestern Mediterranean Basin. Due to the occurrence of strong mesoscale and submesocale dynamics in a context of contrasted and well-defined water masses, the NBF provides the perfect setting for investigating small-scale interactions, associated ageostrophic motion, and energy cascades.

Acknowledgments

The authors acknowledge the financial support of the Direction Générale de l'Armement (DGA, Ministry of Defence) through the PROTEVS project and the Agence Nationale de la Recherche (ANR)-Astrid project DYNED-Atlas (ANR-15-ASMA-0003-01). They thank the technical team at the French Naval Hydrologic and Oceanographic Service (SHOM), the crew of the French Navy ship *Beautemps-Beaupré* for their contribution to the field experiment, and the AVISO center for providing the surface geostrophic currents. Raw data are available on Seanoe data repository at http://doi.org/10.17882/56028.

References

Allen, J. T., Painter, S. C., & Rixen, M. (2008). Eddy transport of Western Mediterranean Intermediate Water to the Alboran Sea. *Journal of Geophysical Research*, *113*, C04024. https://doi.org/10.1029/2007JC004649

Amitai, Y., Lehahn, Y., Lazar, A., & Heifetz, E. (2010). Surface circulation of the eastern Mediterranean Levantine basin: Insights from analyzing 14 years of satellite altimetry data. *Journal of Geophysical Research*, *115*, C10058. https://doi.org/10.1029/2010JC006147

Baird, M. E., & Ridgway, K. R. (2012). The southward transport of sub-mesoscale lenses of Bass Strait Water in the centre of anti-cyclonic mesoscale eddies. *Geophysical Research Letters*, *39*, L02603. https://doi.org/10.1029/2011GL050643

Benzohra, M., & Millot, C. (1995a). Characteristics and circulation of the surface and intermediate water masses off Algeria. *Deep Sea Research Part I: Oceanographic Research Papers*, *42*(10), 1803–1830. https://doi.org/10.1016/0967-0637(95)00043-6

Benzohra, M., & Millot, C. (1995b). Hydrodynamics of an open sea Algerian eddy. *Deep Sea Research Part I: Oceanographic Research Papers*, *42*(10), 1831–1847. https://doi.org/10.1016/0967-0637(95)00046-9

Bosse, A., Testor, P., Houpert, L., Damien, P., Prieur, L., Hayes, D., et al. (2016). Scales and dynamics of submesoscale coherent vortices formed by deep convection in the northwestern Mediterranean Sea. *Journal of Geophysical Research: Oceans*, *121*, 7716–7742. https://doi.org/10.1002/2016JC012144

Brannigan, L. (2016). Intense submesoscale upwelling in anticyclonic eddies. *Geophysical Research Letters*, *43*. https://doi.org/10.1002/2016GL067926, 3360–3369.

Brannigan, L., Marshall, D. P., Naveira Garabato, A. C., Nurser, A. J. G., & Kaiser, J. (2017). Submesoscale instabilities in mesoscale eddies. *Journal of Physical Oceanography*, *47*(12), 3061–3085. https://doi.org/10.1175/JPO-D-16-0178.1

Brassington, G. B. (2009). Estimating surface divergence of ocean eddies using observed trajectories from a surface drifting buoy. *Journal of Atmospheric and Oceanic Technology*, *27*(4), 705–720. https://doi.org/10.1175/2009JTECHO651.1

Chelton, D. B., Schlax, M. G., & Samelson, R. M. (2011). Global observations of nonlinear mesoscale eddies. *Progress in Oceanography*, *91*(2), 167–216. https://doi.org/10.1016/j.pocean.2011.01.002

Cotroneo, Y., Aulicino, G., Ruiz, S., Pascual, A., Budillon, G., Fusco, G., & Tintoré, J. (2016). Glider and satellite high resolution monitoring of a mesoscale eddy in the algerian basin: Effects on the mixed layer depth and biochemistry. *Journal of Marine Systems*, *162*, 73–88. https://doi.org/10.1016/j.jmarsys.2015.12.004

Cresswell, G. R. (1982). The coalescence of two East Australian Current warm-Core eddies. *Science*, *215*(4529), 161–164. https://doi.org/10.1126/science.215.4529.161

Escudier, R., Mourre, B., Juza, M., & Tintoré, J. (2016). Subsurface circulation and mesoscale variability in the Algerian subbasin from altimeter-derived eddy trajectories. *Journal of Geophysical Research: Oceans*, *121*, 6310–6322. https://doi.org/10.1002/2016JC011760

Escudier, R., Renault, L., Pascual, A., Brasseur, P., Chelton, D., & Beuvier, J. (2016). Eddy properties in the Western Mediterranean Sea from satellite altimetry and a numerical simulation. *Journal of Geophysical Research: Oceans*, *121*, 3990–4006. https://doi.org/10.1002/2015JC011371

Estournel, C., Testor, P., Taupier-Letage, I., Bouin, M.-N., Coppola, L., Durand, P., et al. (2016). HyMeX-SOP2: The field campaign dedicated to dense water formation in the northwestern Mediterranean. *Oceanography*, *29*(4), 196–206. https://doi.org/10.5670/oceanog.2016.94

Font, J., Isern-Fontanet, J., & Salas, J. D. J. (2004). Tracking a big anticyclonic eddy in the western Mediterranean Sea. *Scientia Marina*, *68*(3), 331–342. https://doi.org/10.3989/scimar.2004.68n3331

Forryan, A., Allen, J. T., Edhouse, E., Silburn, B., Reeve, K., & Tesi, E. (2012). Turbulent mixing in the eddy transport of Western Mediterranean Intermediate Water to the Alboran Sea. *Journal of Geophysical Research*, *117*, C09008. https://doi.org/10.1029/2012JC008284

Fratantoni, D. M. (2001). North Atlantic surface circulation during the 1990's observed with satellite-tracked drifters. *Journal of Geophysical Research*, *106*, 22,067–22,093. https://doi.org/10.1029/2000JC000730

Fuda, J. L., Millot, C., Taupier-Letage, I., Send, U., & Bocognano, J. M. (2000). XBT monitoring of a meridian section across the western Mediterranean Sea. *Deep Sea Research Part I: Oceanographic Research Papers*, *47*(11), 2191–2218. https://doi.org/10.1016/S0967-0637(00)00018-2

Gaube, P., Chelton, D. B., Samelson, R. M., Schlax, M. G., & O'Neill, L. W. (2014). Satellite observations of mesoscale eddy-induced Ekman pumping. *Journal of Physical Oceanography*, *45*(1), 104–132. https://doi.org/10.1175/JPO-D-14-0032.1

Goncharov, V. V., Yu, A., Chepurin, A., & Aleinik, D. L. (2003). Experimental study of an intrathermocline Mediterranean Water Lens and possibilities of its remote detection. *Isvestya, Atmospheric and Oceanic Physics*, *39*(5), 614–623.

Ioannou, A., Stegner, A., Le Vu, B., Taupier-Letage, I., & Speich, S. (2017). Dynamical evolution of intense Ierapetra eddies on a 22 year long period. *Journal of Geophysical Research: Oceans*, *122*, 9276–9298. https://doi.org/10.1002/2017JC013158

Isern-Fontanet, J., García-Ladona, E., & Font, J. (2006). Vortices of the Mediterranean Sea: An altimetric perspective. *Journal of Physical Oceanography*, *36*(1), 87–103. https://doi.org/10.1175/JPO2826.1

Juza, M., Mourre, B., Renault, L., Gómara, S., Sebastián, K., Lora, S., et al. (2016). SOCIB operational ocean forecasting system and multi-platform validation in the Western Mediterranean Sea. *Journal of Operational Oceanography*, *9*(sup1), s155–s166. https://doi.org/10.1080/1755876X.2015.1117764

Juza, M., Renault, L., Ruiz, S., & Tintoré, J. (2013). Origin and pathways of Winter Intermediate Water in the northwestern Mediterranean Sea using observations and numerical simulation. *Journal of Geophysical Research: Atmospheres*, *118*, 6621–6633. https://doi.org/10.1002/2013JC009231

Kloosterziel, R. C., Carnevale, G. F., & Orlandi, P. (2007). Inertial instability in rotating and stratified fluids: Barotropic vortices. *Journal of Fluid Mechanics*, *583*, 379–412. https://doi.org/10.1017/S0022112007006325

Lazar, A., Stegner, A., & Heifetz, E. (2013). Inertial instability of intense stratified anticyclones. Part 1. Generalized stability criterion. *Journal of Fluid Mechanics*, *732*, 457–484. https://doi.org/10.1017/jfm.2013.412

Le Vu, B., Stegner, A., & Arsouze, T. (2018). Angular momentum eddy detection and tracking algorithm (AMEDA) and its application to coastal eddy formation. *Journal of Atmospheric and Oceanic Technology*, *35*(4), 739–762. https://doi.org/10.1175/JTECH-D-17-0010.1

L'Hégaret, P., Carton, X., Louazel, S., & Boutin, G. (2016). Mesoscale eddies and submesoscale structures of Persian Gulf Water off the Omani coast in spring 2011. *Ocean Science*, *12*(3), 687–701. https://doi.org/10.5194/os-12-687-2016

Li, Q.-Y., Sun, L., & Lin, S.-F. (2016). GEM: A dynamic tracking model for mesoscale eddies in the ocean. *Ocean Science*, *12*(6), 1249–1267. https://doi.org/10.5194/os-12-1249-2016

Lilly, J. M., & Gascard, J.-C. (2006). Wavelet ridge diagnosis of time-varying elliptical signals with application to an oceanic eddy. *Nonlinear Processes in Geophysics*, *13*(5), 467–483. https://doi.org/10.5194/npg-13-467-2006

Mahadevan, A., Thomas, L. N., & Tandon, A. (2008). Comment on "Eddy/wind interactions stimulate extraordinary mid-ocean plankton blooms". *Science*, *320*(5875), 448b–448b. https://doi.org/10.1126/science.1152111

McGillicuddy, D. J. (2016). Mechanisms of physical-biological-biogeochemical interaction at the oceanic mesoscale. *Annual Review of Marine Science*, *8*(1), 125–159. https://doi.org/10.1146/annurev-marine-010814-015606

McGillicuddy, D. J., Anderson, L. A., Bates, N. R., Bibby, T., Buesseler, K. O., Carlson, C. A., et al. (2007). Eddy/wind interactions stimulate extraordinary mid-ocean plankton blooms. *Science*, *316*(5827), 1021–1026. https://doi.org/10.1126/science.1136256

Mcwilliams, J. C. (2013). The nature and consequences of oceanic eddies. In *Ocean modeling in an eddying regime* (pp. 5–15). Washington, DC: American Geophysical Union. https://doi.org/10.1029/177GM03

Meunier, T., Ménesguen, C., Schopp, R., & Le Gentil, S. (2014). Tracer stirring around a meddy: The formation of layering. *Journal of Physical Oceanography*, *45*(2), 407–423. https://doi.org/10.1175/JPO-D-14-0061.1

Millot, C. (1999). Circulation in the Western Mediterranean Sea. *Journal of Marine Systems*, *20*, 423–442. https://doi.org/10.1016/S0924-7963(98)00078-5

Millot, C., Taupierletage, I., & Benzohra, M. (1990). The Algerian eddies. *Earth-Science Reviews*, *20*(1-4), 423–442. https://doi.org/10.1016/0012-8252(90)90003-E

Mkhinini, N., Coimbra, A. L. S., Stegner, A., Arsouze, T., Taupier-Letage, I., & Béranger, K. (2014). Long-lived mesoscale eddies in the eastern Mediterranean Sea: Analysis of 20 years of AVISO geostrophic velocities. *Journal of Geophysical Research: Oceans*, *119*, 8603–8626. https://doi.org/10.1002/2014JC010176

Nof, D., & Dewar, W. K. (1994). Alignment of lenses: Laboratory and numerical experiments. *Deep Sea Research Part I: Oceanographic Research Papers*, *41*(8), 1207–1229. https://doi.org/10.1016/0967-0637(94)90041-8

Paillet, J., Le Cann, B., Carton, X., Morel, Y., & Serpette, A. (2002). Dynamics and evolution of a northern meddy. *Journal of Physical Oceanography*, *32*(1), 55–79. https://doi.org/10.1175/1520-0485(2002)032<0055:DAEOAN>2.0.CO;2

Pascual, A., Pujol, M.-I., Larnicol, G., Le Traon, P.-Y., & Rio, M.-H. (2007). Mesoscale mapping capabilities of multisatellite altimeter missions: First results with real data in the Mediterranean Sea. *Journal of Marine Systems*, *65*(1-4), 190–211. https://doi.org/10.1016/j.jmarsys.2004.12.004

Perez, J. D. S. (2003). Evolution of the open-sea eddy ALGERS'98 in the Algerian Basin with lagrangian trajectories and remote sensing observations. *Journal of Marine Systems*, *43*(3–4), 105–131. https://doi.org/10.1016/j.jmarsys.2003.08.001

Pietri, A., & Karstensen, J. (2018). Dynamical characterization of a low oxygen submesoscale coherent vortex in the eastern North Atlantic Ocean. *Journal of Geophysical Research: Oceans*, *123*, 2049–2065. https://doi.org/10.1002/2017JC013177

Pinot, J.-M., & Ganachaud, A. (1999). The role of winter intermediate waters in the spring-summer circulation of the Balearic Sea: 1. Hydrography and inverse box modeling. *Journal of Geophysical Research*, *104*, 29,843–29,864. https://doi.org/10.1029/1999JC900202

Puillat, I., Taupier-Letage, I., & Millot, C. (2002). Algerian eddies lifetime can near 3 years. *Journal of Marine Systems*, *31*(4), 245–259. https://doi.org/10.1016/S0924-7963(01)00056-2

Pujol, M.-I., Faugère, Y., Taburet, G., Dupuy, S., Pelloquin, C., Ablain, M., & Picot, N. (2016). DUACS DT2014: The new multi-mission altimeter data set reprocessed over 20 years. *Ocean Science*, *12*(5), 1067–1090. https://doi.org/10.5194/os-12-1067-2016

Rio, M.-H., Poulain, P.-M., Pascual, A., Mauri, E., Larnicol, G., & Santoleri, R. (2007). A mean dynamic topography of the Mediterranean Sea computed from altimetric data, in-situ measurements and a general circulation model. *Journal of Marine Systems*, *65*(1-4), 484–508. https://doi.org/10.1016/j.jmarsys.2005.02.006

Robinson, A. R. (1983). *Eddies in marine science* (p. 609). Berlin: Springer Verlag. https://doi.org/10.1007/978-3-642-69003-7

Ruiz, S., Font, J., Emelianov, M., Isern-Fontanet, J., Millot, C., Salas, J., & Taupier-Letage, I. (2002). Deep structure of an open sea eddy in the Algerian Basin. *Journal of Marine Systems*, *33-34*, 179–195. https://doi.org/10.1016/S0924-7963(02)00058-1

Ruiz, S., Pascual, A., Garau, B., Pujol, I., & Tintoré, J. (2009). Vertical motion in the upper ocean from glider and altimetry data. *Geophysical Research Letters*, *36*, L14607. https://doi.org/10.1029/2009GL038569

Salas, J. (2003). Evolution of the open-sea eddy ALGERS'98 in the Algerian Basin with Lagrangian trajectories and remote sensing observations. *Journal of Marine Systems*, *43*, 105–131. https://doi.org/10.1016/j.jmarsys.2003.08.001

Taupier-Letage, I., Puillat, I., Millot, C., & Raimbault, P. (2003). Biological response to mesoscale eddies in the Algerian Basin. *Journal of Geophysical Research*, *108*(C8), 3245. https://doi.org/10.1029/1999JC000117

Testor, P., Send, U., Gascard, J.-C., Millot, C., Taupier-Letage, I., & Béranger, K. (2005). The mean circulation of the southwestern Mediterranean Sea: Algerian gyres. *Journal of Geophysical Research*, *110*, C11017. https://doi.org/10.1029/2004JC002861

Vargas-Yáñez, M., Zunino, P., Schroeder, K., López-Jurado, J. L., Plaza, F., Serra, M., et al. (2012). Extreme Western Intermediate Water formation in winter 2010. *Journal of Marine Systems*, *105-108*, 52–59. https://doi.org/10.1016/j.jmarsys.2012.05.010

Yi, J., Du, Y., He, Z., & Zhou, C. (2014). Enhancing the accuracy of automatic eddy detection and the capability of recognizing the multi-core structures from maps of sea level anomaly. *Ocean Science*, *10*(1), 39–48. https://doi.org/10.5194/os-10-39-2014

Zhong, Y., Bracco, A., Tian, J., Dong, J., Zhao, W., & Zhang, Z. (2017). Observed and simulated submesoscale vertical pump of an anticyclonic eddy in the South China Sea. *Scientific Reports*, *7*(1). https://doi.org/10.1038/srep44011